# PhD Research Proposal: Molecular Level Design of Nanoporous Lyotropic Liquid Crystal Membranes for Aqueous Separations

Advisors: Michael Shirts and Richard Noble

Benjamin J. Coscia

May 6, 2019

# 1 State of the Art

## Commercial Membranes for Small Molecule Separations

More highly selective nanoporous membranes would be useful for performing complex aqueous separations with seawater and various types of wastewater.

- For example, sodium chloride and boron in seawater [1] and organic micropollutants found in municipal and industrial wastewaters [2] represent just a few of the diverse contaminants of water sources.
- By efficiently separating contaminants from feed solutions with highly selective membranes, it is possible to reduce the number of required membrane passes and post-treatment steps needed for a given filtration process [3], thus lowering cost and energy requirements.
- Additionally, one can extract valuable resources from the feed streams. For example, flowback water produced during hydraulic fracturing of shale formations contains dissolved species such as acetate whose extraction has economic value [4].

Reverse osmosis (RO) and nanofiltration (NF) are two prevailing membrane filtration processes that can be used to separate solutes on the order of 1 nm in size and smaller, including ions.

- Both apply hydraulic pressure to the feed solution in order to overcome osmotic pressure and force water and unfiltered components through the membrane.
- RO membranes are typically thin film composite with a porous mechanical support layer and a thin but dense polymer matrix active layer where separations occur.[5]
- RO separates solutes based on the solute's ability to dissolve into and diffuse through the tortuous pathways available in the membrane's dense active layer.
- RO offers high selectivity at the cost of relatively high energy requirements since one must apply hydraulic pressure of up to 100 bar in order to achieve an economical flux [**?**].
- In contrast to RO membranes, NF membranes have explicit pores on the order of 1 nm in size.
- Typically, separations are achieved based on size exclusion and charge exclusion if the membrane's surface has a net charge.
- NF membranes require significantly less applied pressure in order to achieve solute flux comparable to RO.
- Unfortunately, conventional synthesis processes, such as phase-inversion[6] are stochastic in nature which yields pores that are polydisperse in size.[3]
- Pore size polydispersity is detrimental to membrane selectivity

The downfall of RO and NF membranes can be summarized by the well-known permeability-selectivity tradeoff. Namely, it is difficult to increase the permeability of a desired molecular or atomic species, while maintaining the same retention of an undesired species.[3]

## Nanostructured Membranes

Nanostructured membranes attempt to overcome the permeability-selectivity tradeoff through intelligent design at the molecular level.

- Graphene sheets, carbon nanotubes (CNTs) and zeolites are three highly studied nanostructured technologies.

Ultrathin-film graphene and graphene oxide membranes are a very active area of research because they offer potential for extremely high permeability membranes.

- An ideal graphene membrane is a 2D material consisting of a single layer of graphene.[**?**]
- Synthesis of a single layer of graphene at a large scale without introducing defects is a challenge that has not yet been overcome.
- Multilayered graphene membranes are a potentially easier and more scalable technology which has garnered increasing interest in recent years.[**?**, **?**]

Carbon nanotubes (CNTs) have shown promise as aqueous separations membranes due to unprecedentedly fast water transport.[**?**, **?**]

- Practically, dispersing CNTs into a polymer matrix is extremely difficult because they tend to agglomerate due to Van der Waals forces.
- Functionalization of the CNT walls has been heavily investigated as a way to overcome this issue.
- Alignment of the CNTs into an array feasible as a nanoporous membrane presents a further challenge to CNT membranes.[**?**]

Zeolite-coated ceramic membranes offer the potential for permeabilities comparable to ultrafiltration with selectivities as good as NF and RO.

- Zeolites have highly uniform nm-sized crystalline structures with cage-like cavities that allow movement and trapping of small solutes.
- The crystalline frameworks are typically formed by networks of silicon and aluminum each attached to 4 oxygen atoms in a tetrahedral arrangement.
- One can replace the silicon and aluminum atoms via ion exchange in order to control the size of the cavities and hence its molecular-seiving properties.

- A number of studies have tested the permeability and sodium salt rejection of various zeolite membranes, however none have fully overcome the permeability-selectivity tradeoff.
- Most are prone to defects in the crystalline structure.[**?**]

## Lyotropic Liquid Crystal Membranes

Preliminary evidence has shown that cross-linked lyotropic liquid crystal (LLC) membranes can be produced at moderate scale and may be capable of performing highly selective separations.

- LLCs are amphiphilic molecules that have the ability to self-assemble into porous nanostructures[7] that can be cross-linked to create mechanically strong membrane films with periodic uniform-sized pores on the order of 1 nm in diameter [8].
- Since LLC polymer membranes lack an appreciable pore size distribution, they inherently exhibit high selectivity due to their strict molecular weight cut-off (MWCO) [8].
- Additionally, LLC monomers can be salts, and therefore lead to Donnan exclusion of ions in solution.[9]

The feasibility of nanostructured LLC polymer membranes for selective separations has been demonstrated using LLC monomers that form the type 1 bicontinuous cubic ($Q_I$)[10, 11, 12] and the inverted hexagonal ($H_{II}$) [8] phases.

- When separating organic solutes from NaCl, $Q_I$-phase membrane filtration experiments have shown selectivity 2–3 times higher than commercial RO and 6–12 times higher than commercial NF membranes.[4]
- When separating a series of various sized dyes, the $H_{II}$-phase membrane showed complete rejection of dyes bigger than 1.2 nm in size [8].

$Q_I$-phase membranes consist of a tortuous network of three dimensionally interconnected pores that prevent optimal through-plane transport.

- In contrast, the densely packed, non-tortuous and uniform sized pores of $H_{II}$-phase membranes represent the ideal geometry for achieving high solute flux[14].
- However, the hexagonally packed LC domains of the $H_{II}$-phase generally form mutually unaligned domains, which hurts membrane permeability.
- This domain scale misalignment had inhibited further development of this technology, and research efforts were focused on the $Q_I$ phase, whose geometry does not require alignment [15].

Recently, researchers have learned how to macroscopically align the hexagonal domains which has revived research into $H_{II}$-phase LLC polymer membranes.

- In 2014, Feng et al. showed that one can align $Col_h$ domains, a temperature-dependent hexagonal phase created by neat LLC monomers, using a magnetic field with subsequent cross-linking to lock the structure in place[13].
- In 2016, Feng et al. showed that one could also obtain the same result by confining the neat monomer between PDMS or glass substrates since hexagonal mesophases preferentially anchor perpendicular to both surfaces[16].

Unfortunately, reproducing the work of Feng et al. with the hydrated $H_{II}$ phase has been an experimental challenge. Therefore, the primary focus of experimental research efforts has been with the $Q_I$ phase.

## 2 Project Objectives

Our current understanding of the molecular details of LLC membranes' nanostructure is not sufficient to be able to precisely design them for specific separations.

- Dischinger et al. attempted to use an empirical model that correlates the physiochemical properties of the counterion used in a $Q_I$-phase LLC membrane to solute rejection.[17]
- Although their model showed some qualitative agreement with experiment, the quality of fit of their model was limited due to complex solute-membrane interactions that could not easily be modeled.

A molecular-level understanding of structure and transport in LLC polymer membranes, enabled by molecular dynamics (MD) simulations, can provide guidelines to reduce the large chemical space available to design monomers for creation of separation-specific membranes.

- Using a sufficiently accurate molecular model, we can directly observe transport of solutes within LLC membrane nanopores and infer mechanisms.
- Based on this information we will have a much greater capability intelligently design new membranes by screening new liquid crystal monomer designs.
- The principles learned can be implemented and tested experimentally.

There are four primary objectives of this PhD research.

1. Develop techniques to build and understand the nanoscopic structure of LLC membranes.

   A useful molecular-level model should incorporate a detailed picture of the nanoscopic pore structure, which is crucial to understanding the role of monomer structure in solute transport and membrane design. I have created a maximally consistent structural model by comparing simulated X-ray diffraction (XRD) patterns, generated from MD trajectories, to an experimental 2D wide angle X-ray scattering (WAXS) spectrum of a $Col_h$ phase LLC membrane. I have used this model as an example in order to understand the ease with which we can apply our approach to alternate monomers.

2. Determine dominant solute-membrane interactions that give rise to transport mechanisms.

   I observed the transport of a relatively large set of small polar solutes placed within the $H_{II}$ phase membrane nanopores. I analyzed the time series of each solute's position in addition to directly measuring the physical interactions, such as hydrogen bonding and ion coordination, between solutes and LLC monomers.

3. Create a stochastic model which can project long timescale transport behavior.

   I will combine my qualitative knowledge of the solute transport mechanisms with simulation data in order to inform a stochastic model. This model should closely reproduce the properties of the time series that we observe in our simulations. Due to the low computational cost of a stochastic model relative to MD simulations, I will be able to forecast long timescale transport behavior and make well-converged predictions of macroscopic transport properties.

4. Adapt the same analysis to the $Q_I$ phase.

   Over the course of this project, experimental research surrounding LLC membranes has shifted nearly all focus towards the $Q_I$ phase due to its more facile synthesis. Although most of my work has been applied to the $H_{II}$ phase, much of the same analyses can be applied to the $Q_I$ phase. The biggest challenge will be adapting my techniques to its more complex three dimensional geometry.

# 3 Progress to Date

**Objective 1:** Build and understand the nanoscopic structure of the $H_{II}$ phase (**Complete**)

Our first task was to develop a procedure for building and equilibrating an atomistic LLC membrane system (see Figure 1).

- We built a monoclinic unit cell consisting of four pores.
- Each pore is composed of monomer columns, where each column consists of 20 monomers stacked on top of each other so that the phenyl groups are coplanar with each other and the $xy$ plane.
- The columns are oriented so that the hydrophilic monomer head groups face towards the pore center.
- We did not add any water to the initial configuration because we compared our structure to experimental data for a system claimed to be synthesized dry.
- We equilibrated the unit cell using a series of simulations with head groups held in place by position restraints.
- We gradually reduce the force constant of the position restraints until the system is completely unrestrained.

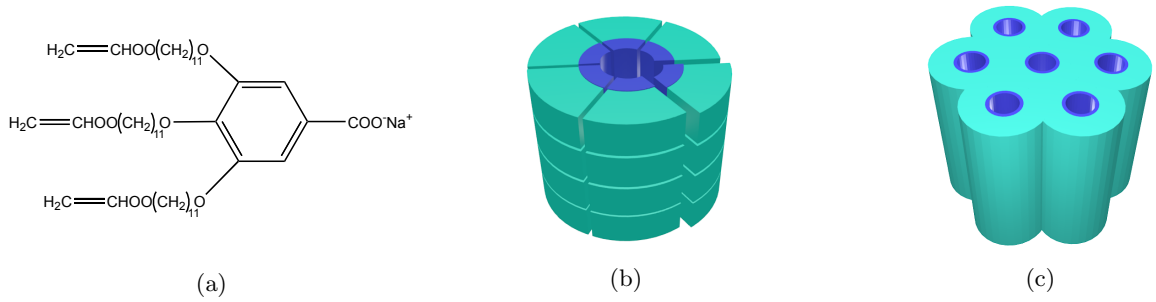


(a) (b) (c)

Figure 1: (a) The LLC monomer Na-GA3C11 exhibits wedge-like character. (b) Monomers stack on top of each other to create columns with short range order, then assemble into pores with hydrophilic head groups (blue) facing towards the pore center. (c) The pores assemble into hexagonally packed columnar mesophases.

- We carried out 400 ns equilibration simulations.

We tested a number of different initial column architectures.

- We stacked monomers in parallel displaced and sandwiched configurations, two possible $\pi$-$\pi$ stacking modes.[**?**]
- We also varied the initial distance between stacked monomers, $d$.
- We chose values of 3.7 Å, based on experimental WAXS measurements, as well as 5 Åas a test of its sensitivity.

Our model's geometry is most consistent with experiment for systems built with 5 columns per pore and monomers initially stacked 3.7 Å apart (see Figure 2).

- We equilibrated systems with 4, 5, 6, 7 and 8 columns per pore.
- The pore spacing of 5 column-per-pore systems agree well with experiment.
- 6 column-per-pore systems built with $d = 5$ Å appear to yield an experimentally consistent pore spacing however, the equilibrated distance between stacked monomers stay close to 5 Å which is inconsistent with experiment.
- In general, the equilibrated distance between monomers stays close to its initial value.

We further validated the structure of our molecular model by verifying its consistency with five major reflections present in the experimental WAXS pattern.

- The five major reflections and the structural features leading to them are summarized and described in the caption of Figure 3.
- Using MD trajectories, we simulated X-ray diffraction (XRD) patterns that we could compare to the WAXS data by taking the appropriate cross-section of the time-averaged 3D structure factor.

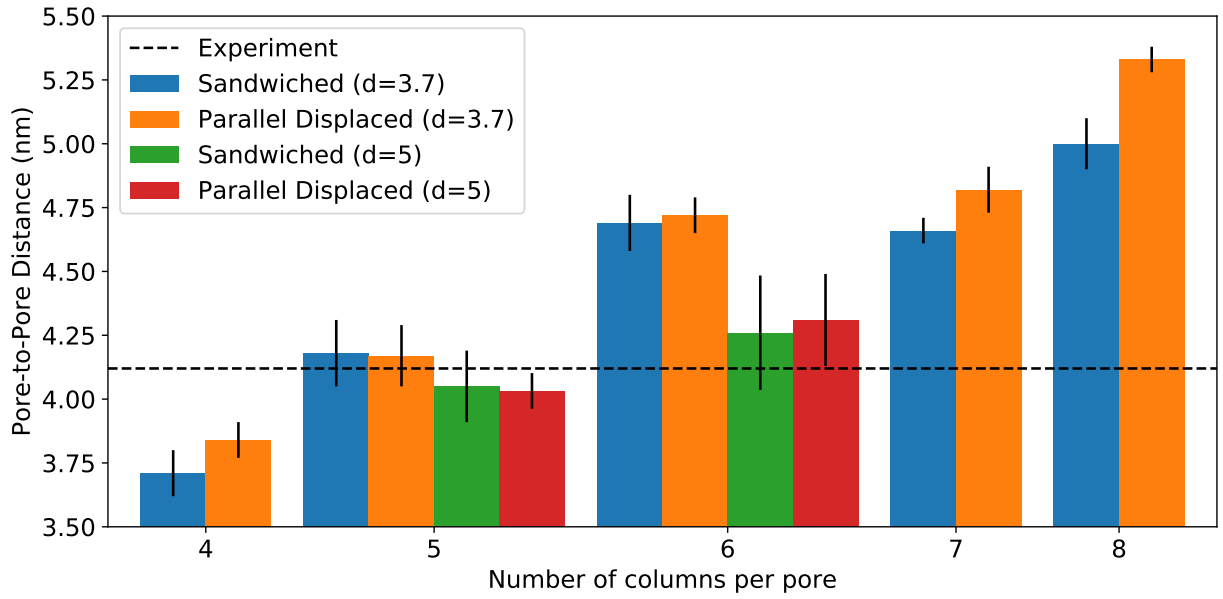


Figure 2: Systems with 5 columns per pore have equilibrated pore spacings closest to the experimental value of 4.12 nm. The equilibrated pore spacing of the model increases as the number of columns in each pore increases.

- None of the models simulated to this point could reproduce R-double.

It is necessary to add a small amount of water to our model in order to fully reproduce all features of the WAXS pattern (see Figure 3b).

- We built our most experimentally consistent structure in the parallel displaced configuration with 1 wt% water added to the pores.
- This is the only configuration that gives rise to the R-double feature.
- R-double appears because vertically adjacent monomer head groups hydrogen bond with shared water molecules, causing them to be drawn closer together.
- When multiple pairing interactions occur in series along the same pore axis, the center of masses of the pairs are spaced apart at twice the $\pi$-stacking distance.
- The necessity of water in our model suggests that the membrane synthesized by Feng et al. was slightly hydrated due to water molecules leached from surroundings by the hydroscopic monomers.

On the timescales that we can reasonably simulate, our model exhibits slow dynamics.

- Consequently, there are very few uncorrelated frames in our trajectories which leads to noise in the simulated XRD patterns.
- We can overcome this issue by combining the structure factors generated from an ensemble of trajectories produced starting from an ensemble of uncorrelated initial configurations.

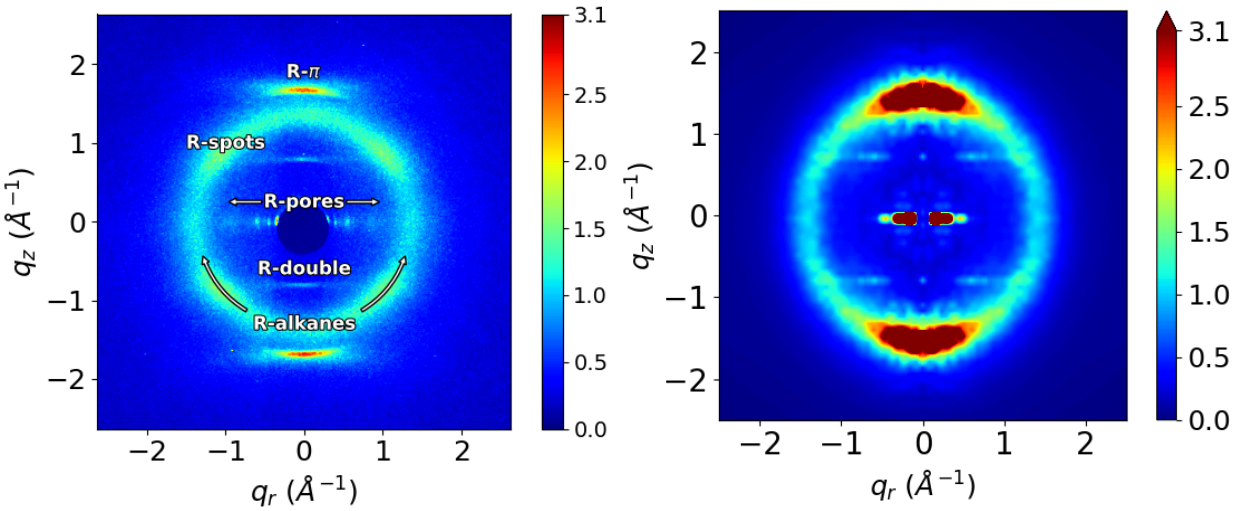


(a) Experiment

(b) Simulation

Figure 3: (a) 2D-WAXS gives details about repeating features on the order of angstroms. Our explanations for each of the 5 major reflections present are as follows: (R-$\pi$) Aromatic head groups $\pi - \pi$ stack 3.7 Å apart. (R-double) Monomer head groups associate into pairs by hydrogen bonding with a shared water molecule. (R-alkanes) Alkane chain tails pack 4.5 Å apart. (R-spots) Monomer tails pack hexagonally. (R-pores) The pores are spaced 4.12 nm apart and pack hexagonally. (b) We obtain a maximally consistent match between simulated XRD patterns and experimental WAXS data when we build systems in the parallel displaced configuration with 1 wt % water included in the pores.

The composition of the pores does not change regardless of which initial configuration we study.

- In Figure 4, we plot the radial density of various monomer components as a function of distance from the pore centers.
- All are qualitatively similar meaning that a solute placed in any of these systems should experience a similar chemical environment.
- Although we will move forward with our most promising configuration, this is an important finding since it implies that we do not need to apply the same level of rigor when screening new monomers.

## **Objective 2:** *Determine transport mechanisms* (**Complete**)

We added additional water to our most experimentally consistent structural model in order to create a higher water content $H_{II}$ phase model.

- There have been a range of reported water contents used to form the $H_{II}$ phase with this particular monomer.
- Although Resel et al. commented that the system is likely already fully hydrated at 7 wt % water with additional water trapped in defects between mesophases.[**?**]
- Therefore, we built two systems with 5 and 10 wt% water.

We observed that water partitions into the distal tail region.

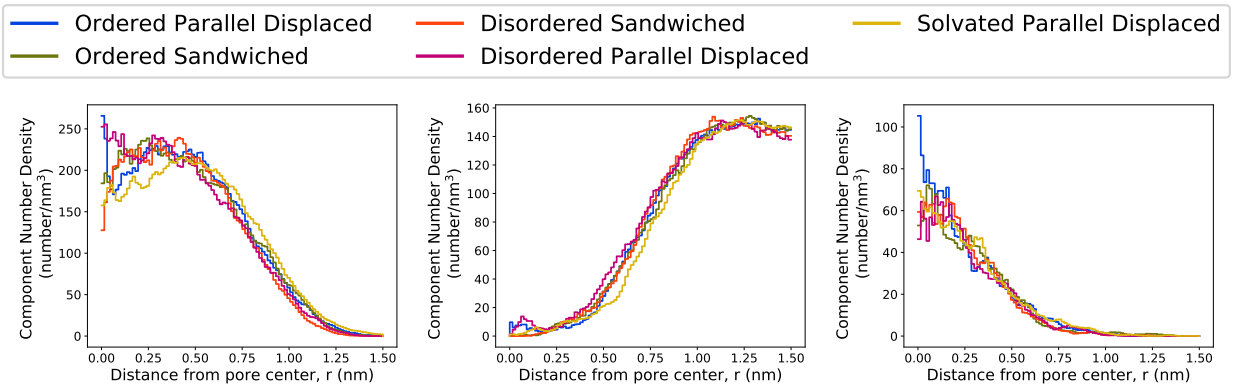


(a) Head Groups (b) Tails (c) Sodium Ions

Figure 4: In all cases, the component radial distribution functions are similar. They exhibit a composition gradient transitioning from the hydrophilic to the hydrophobic regions. The biggest differences are at r=0 where noise is higher due to decreased sampling. The center of the pore is not hollow, but contains sodium ions and head groups, even when the system is solvated. This architecture may impede transport in the real system in a chemically-dependent manner. The solvated system has a lower density of head groups near the pore center which is likely due to the swelling that is necessary in order to fit water molecules in the pore region.

- We define the distal tail region to be any radial distance greater than 1.5 nm from any pore center.
- There is approximately a 3:2 ratio of water in the pores to water in the distal tails.
- Due to the wedge shape of the monomers, the distal tail region has a relatively low density leaving space for water molecules to fill.

The pores of the $H_{II}$ phase are primarily a mixture of water and sodium ions.

- The maximum density of head groups occurs 0.45 and 0.65 nm from the pore center in the 5 and 10 wt% water systems respectively (see Figure 5).
- There are almost no head groups occupying the pore center.

Water and sodium transport is significantly faster in the less crowded 10 wt% water pores.

- The mean squared displacement (MSD) of water is about 51 times higher and the MSD of sodium is about 49 times higher compared to the 5 wt% system.
- In general we observe similar solute transport mechanisms in the 5 and 10 wt% water systems but on different time scales.

We observed transport of 20 different small polar solutes in the pores of our model.

- We created a separate initial configuration for each solute studied and placed 6 solutes, equally spaced in $z$, in each nanopore.
- After a brief equilibration, we allowed the solutes to simulate for 1 microsecond.

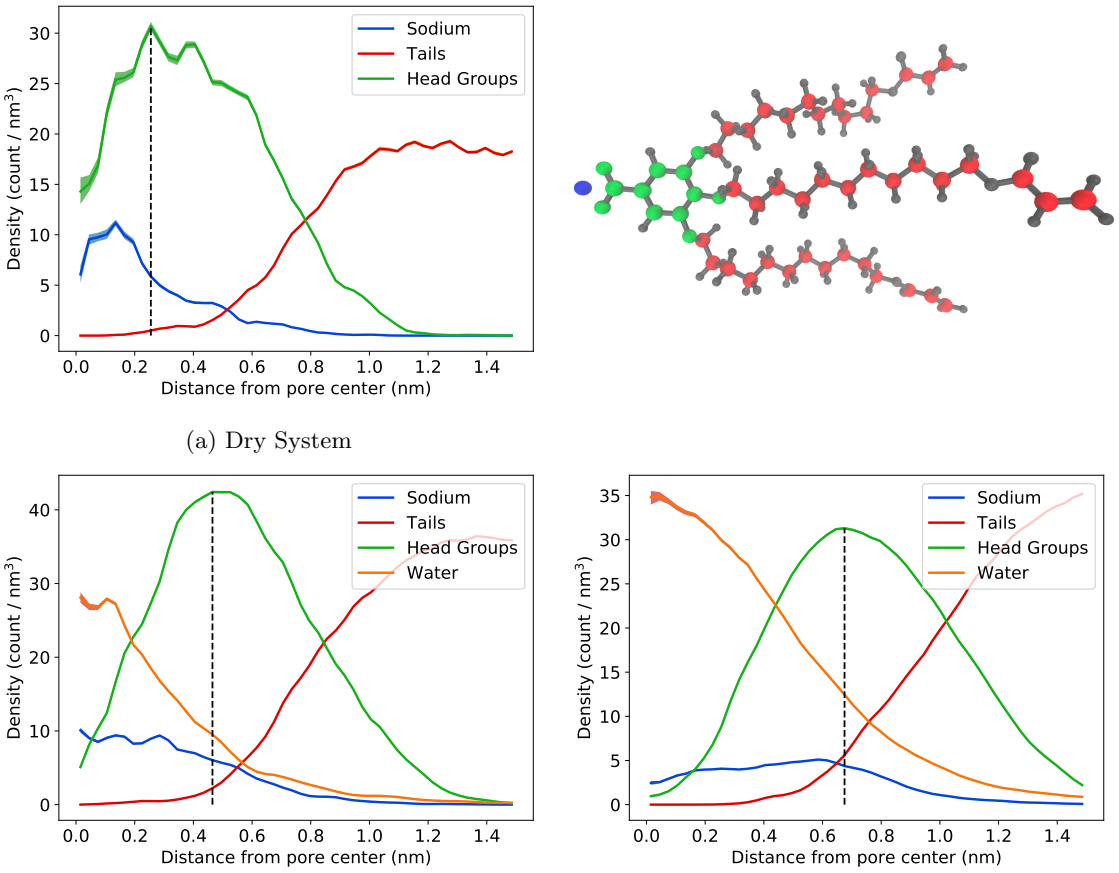


(a) Dry System

(b) 5 wt% water

(c) 10 wt% water

Figure 5: The radial densities of various monomer components paint a picture of the pore topology where the pore centers are primarily composed of water and sodium ions. The monomer groups labeled in each plot correspond to the color-coded monomer pictured in the upper right corner of the figure. All RDFs represent the number of atoms located at a given distance from the pore center normalized by the volume of the annular bin to which they belong. (a) In the dry system, the density of head groups and sodium ions are highest within 0.25 nm of the pore center. (b) In the 5 wt % system, monomer head groups retreat about 0.2 nm radially in order to make room for water molecules. (c) Monomers in the 10 wt % system retreat an additional 0.2 nm to make room for more water.

The solute MSDs are not a monotonic function of solute size.

- In Figure 6a, we plotted the average MSD of each solute.
- In Figure 6b, we plotted solute MSDs against their molecular radius.
- We also plotted theoretical curves which illustrate the expected MSD of each solute if they were to travel unhindered.
- We ensured that the Stokes-Einstein equation with the correction factor of Gierer and Wirtz[**?**] passed through methanol in order to give an approximate frame of reference.
- Methanol is small and therefore can travel relatively unhindered compared to all other solutes.

- The correction factor attempts to include the effects of microfriction that begin to play a role when solute size becomes on the order of solvent size.
- The theoretical line can be used as an approximate boundary between subdiffusive, Brownian and superdiffusive behavior.

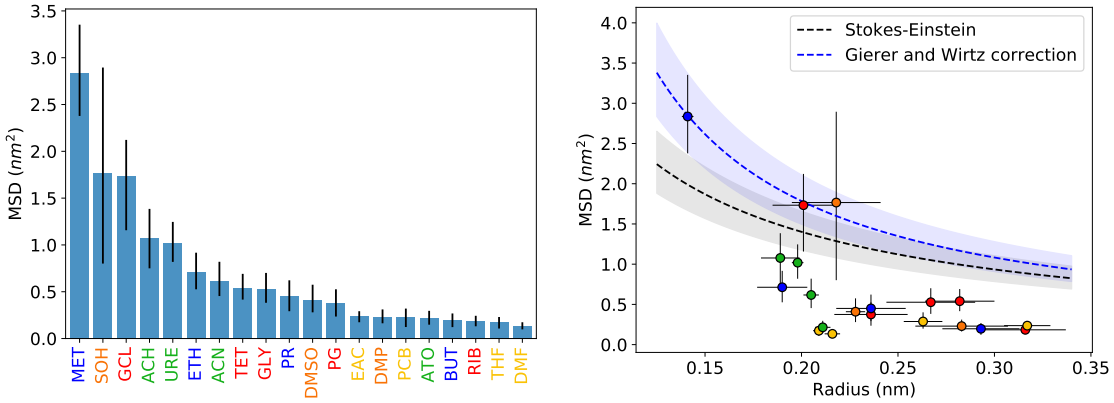


(a) 10 wt % water

(b) 10 wt % water

Figure 6: The MSDs of solutes in the 5 wt % water system (a) are significantly smaller than those of the solutes in the 10 wt % water system (b). The MSDs are not a monotonic function of molecular size (c and d). A significant number of solute MSDs fall below the theoretical lines predicted by the Stokes-Einstein equation and Gierer and Wirtz' corrected Stokes-Einstein equation.

Intermittent hops between long periods of entrapment lead to subdiffusive solute transport behavior.

- As Figure 6b implies, most solutes move significantly slower than expected.
- In Figure 7a, we've plotted the $z$-direction trajectory of three ethanol molecules.
- Typically, long periods of entrapment occur when ethanol molecules are far from the pore center, while there is a much greater degree of mobility close to the pore center.
- The MSD curve averaged over all ethanol trajectories is shown in Figure 7b.
- The curve is sub-linear and thus subdiffusive.

We observe three mechanisms of entrapment that are responsible for subdiffusive behavior.

1. As already demonstrated in Figure 7a, solutes that drift away from the pore center can become entangled in the monomer tails.
2. Many of the solutes we studied are capable of donating hydrogen bonds to monomer head groups and thus are prone to temporary immobilization through this interaction.
3. Because all solutes are polar, they have regions of concentrated electron density, modeled as partial charges, which can associate with sodium ions partially bound to monomer head groups.

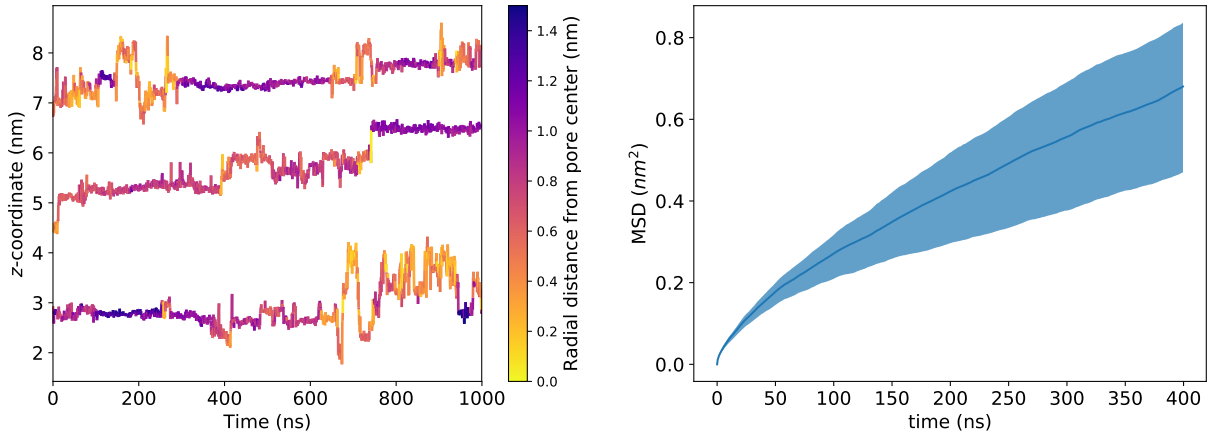


(a) (b)

Figure 7: All solutes show subdiffusive transport behavior inside the membrane's nanopores, similar to that exhibited by ethanol. (a) The $z$-coordinate trace of 3 representative ethanol COMs shows clear periods of entrapment separated by hops. In general, the longest dwell times occur when solutes are situated far from the pore center and the hops occur when solutes are close to the pore center. (b) The time-averaged MSD of ethanol is sub-linear which suggests transport is governed by an anomalous subdiffusion process.

Due to the crowded environment among the monomer tails, solutes generally move faster in the less dense pore region.

- Figure 8a shows that this is the case for all solutes.
- Hops made in the pore region are on average 59 % larger than those made outside the pore region.

However, time spent in the pore region does not necessarily result in a high MSD.

- For example, ribose spends the largest fraction of time in the pore region, but has the fifth lowest hop frequency and the third lowest average MSD (see Figures 8b and 8c).

The frequency with which solutes donate hydrogen bonds to monomer head groups is related to the number of hydrogen bond donating atoms as well as their identity.

- The percentage of solutes actively participating in at least one hydrogen bond with a head group each frame descends as the number of hydroxyl groups decreases.
- Solutes with many hydroxyl groups, such as ribose, tetrose and glycerol, can donate multiple hydrogen bonds to monomer head groups simultaneously.
- When one hydrogen bond is broken, other hydrogen bonds work to hold the solute in place, which allows broken hydrogen bonds to reform.
- Solutes that containing sulfur and nitrogen atoms in place of oxygen atoms hydrogen bond less frequently since they are less electronegative elements.

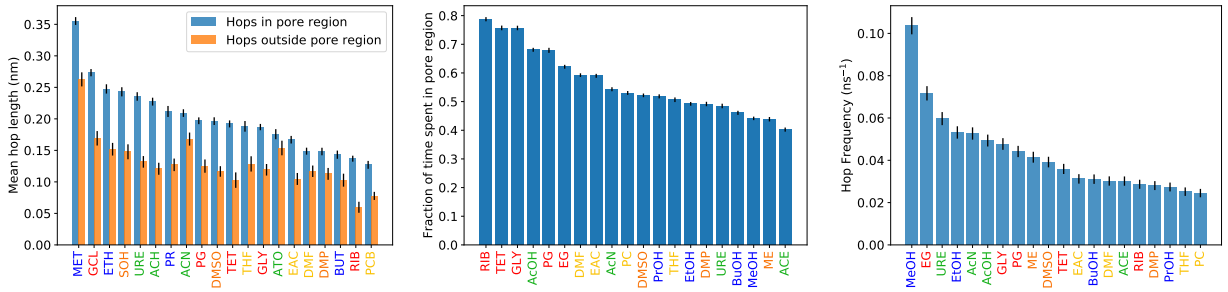


(a) (b) (c)

Figure 8: (a) Hops made in the pore region of the 10 wt% water system are, on average, 59 % larger than those made outside the pore region. The trend in hop lengths is similar to the trend in MSDs shown in Figure 6a implying that solutes which make consistently larger hops have higher MSDs. The fraction of time spent by a solute in the pore region (b) does not necessarily lead to more frequent hopping (c). For example, ribose spends the largest fraction of time in the pore region, yet performs the the fifth lowest number of hops.

- The lifetime of hydrogen bonds follows nearly the same trend. Hydrogen bonds of solutes that hydrogen bond more frequently last longer.

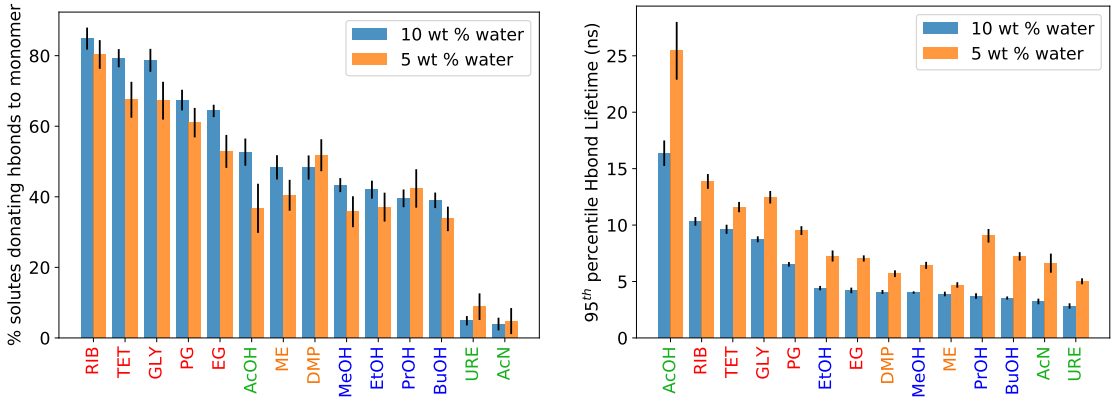


(a) (b)

Figure 9: (a) Solutes capable of donating hydrogen bonds to monomer head groups do so to varying degrees. The reported percentages represent unique solute-monomer hydrogen bonds. Individual solutes that hydrogen bond with multiple head groups simultaneously are only counted once. (b) The lifetime of individual hydrogen bonds appears correlated to the percentage of solutes involved in hydrogen bond interactions. Hydrogen bond lifetimes tend to be longer for solutes that hydrogen bond frequently. Note that solutes incapable of donating hydrogen bonds are omitted from this figure.

Solutes with carbonyl groups tend to associate with sodium ions most frequently.

- Nearly all of the most coordinated solutes contain a carbonyl group (except for DMSO which has an analogous sulfinyl group).
- There is a significant drop in sodium ion association for solutes that do not contain carbonyl groups or multiple hydroxyl groups to compensate (see Figure 10a).

- The corresponding dwell times follow a similar trend, however the dwell times of highly coordinated solutes with multiple hydroxyl groups are generally lower since association between hydroxyl groups and sodium is apparently a weaker interaction (Figure 10b).

- Solutes with nitrogen atoms adjacent to the carbonyl groups tend to associate with sodium ions significantly more.

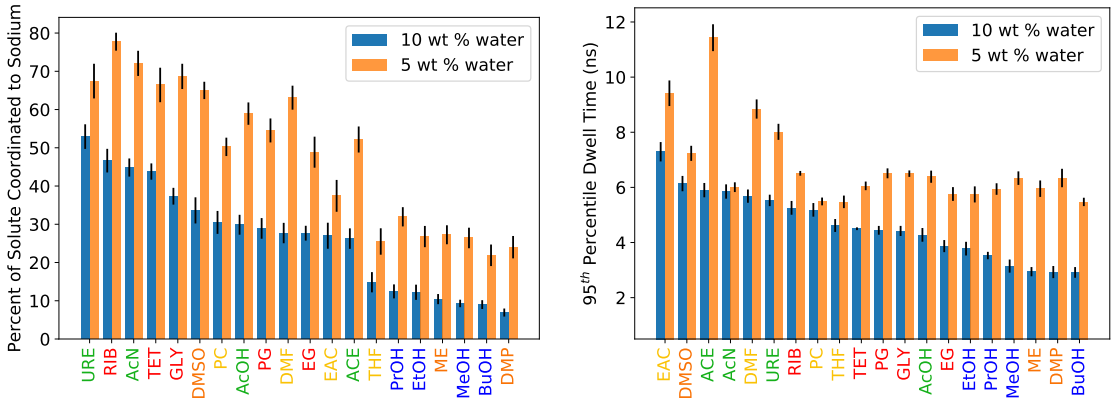


(a) (b)

Figure 10: (a) Solutes, especially those with carbonyl groups, spend a significant fraction of time coordinated to sodium ions. (b) The length of time a solute-sodium pairs spends associated tends to be higher for pairs that associate more frequently.

**Objective 3:** *Create a stochastic model* (**In Progress**) We are in the process of developing the theory required to build a stochastic model.

The distribution of dwell times is power law distributed.

The distribution of hop lengths is approximately Gaussian

The model will likely have a radial dependence.

**Objective 4:** *Apply analyses to $Q_I$ phase* (**In Progress**)

Paralleling our work on the $H_{II}$ phase, our first task was to build a suitable unit cell representation of the $Q_I$ phase.

- Unfortunately, the true space group of the $Q_I$ phase that we are studying is unknown.

- Experimental diffraction has narrowed down the possible bicontinuous cubic configurations to the Ia3d and Pn3m space groups.

- Therefore, we will build both types of unit cells and search for cues that can be used to differentiate them experimentally.

We have developed procedures to build both Ia3d and Pn3m unit cells.

- To our knowledge, nobody has ever built an atomistic bicontinuous cubic phase system without the aid of self-assembly.

- Self-assembly can be a long process, especially for fully atomistic systems.
- Instead, we used known analytical equations that describe the surface of these systems in order to place monomers into a unit cell.
- Monomers are placed perpendicular to the surface in random locations that don't overlap. One can control the pore size by translating monomers perpendicular to the surface at the point where they are attached.

# 4 Timeline for Completion of Objectives

A schematic of the estimated timeline that will be followed for the completion of tasks pertinent to finishing all objectives is given in Table 1.

- Simulations required to study the structure of the bicontinuous cubic phase will be run in parallel while working out the details of our stochastic model of transport in the $H_{II}$ phase.
- Simulations and analysis required for $Q_I$ phase solute transport studies analogous to those of Objective 2 will be carried out throughout Fall 2019.
- Finalization of code documentation and application of a stochastic model to the $Q_I$ phase will be finished by May 2020

TABLE 1 Estimated Timeline for Completion of Objectives

| | |
|---|---|
| August 2019 | Complete Stochastic Model for $H_{II}$ phase |
| September 2019 | Finalize $Q_I$ phase structure |
| January 2020 | Finish transport study of $Q_I$ phase |
| April 2020 | Complete code documentation |
| April 2020 | Finish application of stochastic model to $Q_I$ phase |
| May 2020 | PhD Defense |

# 5 Resource Requirements

The remainder of our work will require the use of high performance computing (HPC) resources.

- We will continue using Bridges, an XSEDE resource as well as Summit, a supercomputer located at CU Boulder.

# References


[1] C. Fritzmann, J. Lwenberg, T. Wintgens, and T. Melin, "State-of-the-Art of Reverse Osmosis Desalination," *Desalination*, vol. 216, pp. 1–76, Oct. 2007.

[2] R. P. Schwarzenbach, B. I. Escher, K. Fenner, T. B. Hofstetter, C. A. Johnson, U. v. Gunten, and B. Wehrli, "The Challenge of Micropollutants in Aquatic Systems," *Science*, vol. 313, pp. 1072–1077, Aug. 2006.

[3] J. R. Werber, C. O. Osuji, and M. Elimelech, "Materials for Next-Generation Desalination and Water Purification Membranes," *Nat. Rev. Mater.*, vol. 1, p. 16018, May 2016.

[4] S. M. Dischinger, J. Rosenblum, R. D. Noble, D. L. Gin, and K. G. Linden, "Application of a Lyotropic Liquid Crystal Nanofiltration Membrane for Hydraulic Fracturing Flowback Water: Selectivity and Implications for Treatment," *J. Membr. Sci.*, vol. 543, pp. 319–327, Dec. 2017.

[5] B.-H. Jeong, E. M. V. Hoek, Y. Yan, A. Subramani, X. Huang, G. Hurwitz, A. K. Ghosh, and A. Jawor, "Interfacial Polymerization of Thin Film Nanocomposites: A New Concept for Reverse Osmosis Membranes," *J. Membr. Sci.*, vol. 294, pp. 1–7, May 2007.

[6] C. A. Smolders, A. J. Reuvers, R. M. Boom, and I. M. Wienk, "Microstructures in Phase-Inversion Membranes. Part 1. Formation of Macrovoids," *J. Membr. Sci.*, vol. 73, pp. 259–275, Oct. 1992.

[7] R. C. Smith, W. M. Fischer, and D. L. Gin, "Ordered Poly(p-phenylenevinylene) Matrix Nanocomposites via Lyotropic Liquid-Crystalline Monomers," *J. Am. Chem. Soc.*, vol. 119, no. 17, pp. 4092–4093, 1997.

[8] M. Zhou, T. J. Kidd, R. D. Noble, and D. L. Gin, "Supported Lyotropic Liquid-Crystal Polymer Membranes: Promising Materials for Molecular-Size-Selective Aqueous Nanofiltration," *Adv. Mater.*, vol. 17, pp. 1850–1853, Aug. 2005.

[9] F. G. Donnan, "Theory of Membrane Equilibria and Membrane Potentials in the Presence of Non-Dialysing Electrolytes. a Contribution to Physical-Chemical Physiology," *J. Membr. Sci.*, vol. 100, pp. 45–55, Mar. 1995.

[10] E. S. Hatakeyama, C. J. Gabriel, B. R. Wiesenauer, J. L. Lohr, M. Zhou, R. D. Noble, and D. L. Gin, "Water Filtration Performance of a Lyotropic Liquid Crystal Polymer Membrane with Uniform, Sub-1-Nm Pores," *J. Membr. Sci.*, vol. 366, no. 1-2, pp. 62–72, 2011.

[11] E. S. Hatakeyama, B. R. Wiesenauer, C. J. Gabriel, R. D. Noble, and D. L. Gin, "Nanoporous, Bicontinuous Cubic Lyotropic Liquid Crystal Networks via Polymerizable Gemini Ammonium Surfactants," *Chem. Mater.*, vol. 22, pp. 4525–4527, Aug. 2010.

[12] B. M. Carter, B. R. Wiesenauer, E. S. Hatakeyama, J. L. Barton, R. D. Noble, and D. L. Gin, "Glycerol-Based Bicontinuous Cubic Lyotropic Liquid Crystal Monomer System for the Fabrication of Thin-Film Membranes with Uniform Nanopores," *Chem. Mater.*, vol. 24, pp. 4005–4007, Nov. 2012.

[13] X. Feng, M. E. Tousley, M. G. Cowan, B. R. Wiesenauer, S. Nejati, Y. Choo, R. D. Noble, M. Elimelech, D. L. Gin, and C. O. Osuji, "Scalable Fabrication of Polymer Membranes with Vertically Aligned 1 nm Pores by Magnetic Field Directed Self-Assembly," *ACS Nano*, vol. 8, pp. 11977–11986, Dec. 2014.

[14] M. Matyka, A. Khalili, and Z. Koza, "Tortuosity-Porosity Relation in Porous Media Flow," *Phys. Rev. E*, vol. 78, p. 026306, Aug. 2008.

[15] M. Zhou, P. R. Nemade, X. Lu, X. Zeng, E. S. Hatakeyama, R. D. Noble, and D. L. Gin, "New Type of Membrane Material for Water Desalination Based on a Cross-Linked Bicontinuous Cubic Lyotropic Liquid Crystal Assembly," *J. Am. Chem. Soc.*, vol. 129, pp. 9574–9575, Aug. 2007.

[16] X. Feng, S. Nejati, M. G. Cowan, M. E. Tousley, B. R. Wiesenauer, R. D. Noble, M. Elimelech, D. L. Gin, and C. O. Osuji, "Thin Polymer Films with Continuous Vertically Aligned 1 nm Pores Fabricated by Soft Confinement," *ACS Nano*, vol. 10, pp. 150–158, Jan. 2016.

[17] S. M. Dischinger, M. J. McGrath, K. R. Bourland, R. D. Noble, and D. L. Gin, "Effect of Post-Polymerization Anion-Exchange on the Rejection of Uncharged Aqueous Solutes in Nanoporous, Ionic, Lyotropic Liquid Crystal Polymer Membranes," *J. Membr. Sci.*, vol. 529, pp. 72–79, May 2017.